Author Manuscript

Author Manuscript

Author Manuscript

Author Manuscript

HHS Public Access

Author manuscript

Nat Chem Biol. Author manuscript; available in PMC 2012 March 01.

Published in final edited form as:

Nat Chem Biol. ; 7(9): 602–609. doi:10.1038/nchembio.624.

Amyloid-β Forms Fibrils by Nucleated Conformational Conversion of Oligomers

Jiyong Lee, **Elizabeth K. Culyba**, **Evan T. Powers**, and **Jeffery W. Kelly***

Departments of Chemistry and Molecular and Experimental Medicine, The Scripps Research Institute and The Skaggs Institute for Chemical Biology. 10550 North Torrey Pines Road, La Jolla, CA 92037, USA.

Abstract

Aβ amyloidogenesis is reported to occur via a nucleated polymerization mechanism, if so the energetically unfavorable oligomeric nucleus should be very hard to detect. However, many laboratories have detected early non-fibrillar Aβ oligomers without observing amyloid fibrils, suggesting a mechanistic revision may be needed. Herein, we introduce Cys-Cys-$A\beta_{1\text{-}40}$ that cannot bind to the latent fluorophore FlAsH as a monomer, but is capable of binding FlAsH as an non-fibrillar oligomer or as a fibril, rendering the conjugates fluorescent. FlAsH monitoring of Cys-Cys-$A\beta_{1\text{-}40}$ aggregation provides compelling evidence that $A\beta_{1\text{-}40}$ very rapidly and efficiently forms spherical oligomers *in vitro* (85% yield) that are kinetically competent to slowly convert to amyloid fibrils by a nucleated conformational conversion mechanism (seedable). Moreover, this methodology demonstrated that plasmalogen ethanolamine vesicles eliminate the proteotoxicity-associated oligomerization phase of Aβ amyloidogenesis, while allowing fibril formation, rationalizing how low plasmalogen ethanolamine levels in the brain are epidemiologically linked to Alzheimer's disease.

Alzheimer's disease (AD) is an aging-associated, progressive neurodegenerative disorder leading to synapse and neuronal loss in the cerebral cortex and subcortical regions of the brain [1-3]. Proteotoxicity linked to the presence of amyloid-β (Aβ) oligomers, as well as intracellular hyperphosphorylated tau aggregates, is thought to cause the neurodegeneration characteristic of AD through a mechanism(s) that remains unclear[1,4-6]. Aβ (39 – 43 amino acids in length) arises from β- and γ-secretase cleavage of the amyloid precursor protein (APP) in the cellular secretory and endocytic pathways[7]. Aβ oligomers of many different sizes and shapes have been reported, such as dimers[6,8], tetramers[9,10], nonamers and dodecamers (Aβ*56)[11], Aβ-derived diffusible ligands (ADDL)[12] and micelles[13,14]. An AD mouse model harboring the E22Δ $A\beta_{1\text{-}40}$ mutation capable of forming oligomers but not fibrils was recently shown to develop cognitive deficits[15].

Users may view, print, copy, download and text and data- mine the content in such documents, for the purposes of academic research, subject always to the full Conditions of use: http://www.nature.com/authors/editorial_policies/license.html#terms

*jkelly@scripps.edu.

AUTHOR CONTRIBUTIONS J. L. designed and performed experiments, analyzed data and wrote the paper. E.K.C. performed experiments and wrote the paper. E.T.P and J.W.K. designed experiments, analyzed data and wrote the paper.

COMPETING FINANCIAL INTERESTS STATEMENT JWK is a cofounder, paid consultant and a shareholder of FoldRx Pharmaceuticals (Pfizer) and Proteostasis Therapeutics, Inc.

Author Manuscript Author Manuscript Author Manuscript Author Manuscript

Monomeric $A\beta_{1-40}$ has been reported to aggregate by a nucleated polymerization mechanism *in vitro*[16-19], wherein rate-limiting formation of an oligomeric nucleus (associated with a lag phase in thioflavin T (ThT) fluorescence) is followed by a rapid growth phase during which monomers add to the ends of the nuclei or growing fibrils (associated with a rapid increase in ThT fluorescence) until the concentration of monomers reaches the so-called critical concentration, the minimal concentration leading to fibril growth[16,17]. Because the nucleus is the highest energy species in this type of aggregation reaction, its concentration should be very low at all times in the aggregation time course. In contrast, monomers and fibrils should be easily detectable early in the aggregation time course. Many laboratories have reported oligomer formation in the absence of detectable amyloid fibril formation early in Aβ amyloidogenesis time courses [13,14], however few have quantified the extent of oligomer formation or assessed whether the oligomers are kinetically competent to form amyloid fibrils. Hence, the oligomers have been often dismissed from a mechanistic perspective as minor species or off-pathway aggregates.

ThT binding, affording fluorescence, insensitively detects Aβ oligomers, at best[20,21]. In contrast, data from size-exclusion chromatography, dynamic light scattering, analytical ultracentrifugation, electron microscopy, and atomic force microscopy all provide strong evidence for the formation of oligomers before the appearance of fibrils in Aβ amyloidogenesis time courses [6,8-14,22] However, the vast majority of scientists still monitor Aβ aggregation reactions using ThT fluorescence because of the availability of fluorescence capacity in most laboratories, even though this approach is largely blind to oligomer formation. Thus, we set out to generate split FlAsH binding site-based Aβ aggregation sensors that reliably and differentially detect both oligomers and fibrils using the FlAsH fluorescence approach discovered by the Tsien laboratory[23].

The FlAsH fluorescence approach has been employed previously to monitor protein tertiary and quaternary structure formation *in vitro* and/or *in vivo*[24-28]. A tetra-Cys motif incorporated into the prion protein was used to detect the difference between the normal cellular conformation (PrP^{c}) and a beta-sheet-rich conformation of the prion protein (PrP^{sc})[24]. Recent studies suggest that the FlAsH tetra-Cys recognition sequence can be split, i.e., Cys-Cys can be placed in separate regions of one protein to report on protein folding or in distinct sequences to detect protein-protein interactions[25-28]. Intramolecular β-sheet folding brings two strands each containing two Cys residues into proximity, creating a non-contiguous tetra-Cys FlAsH binding site rendering the conjugate fluorescent[26]. Moreover, the Schepartz laboratory has utilized *in trans* FlAsH binding site creation to detect coiled-coil dimerization[25]. Webber et al. published that p53 oligomerization can be monitored by incorporating a split tetra-Cys motif in two different quaternary structural interfaces[28]. However, a high level of non-specific binding of FlAsH to p53 lacking split FlAsH sites was observed, suggesting further optimization is required for detecting quaternary structural changes in p53.

Notably, the split tetra-Cys approach has not yet been applied to monitor protein aggregation. Since Aβ amyloid fibrils are established to form in-register, parallel, cross-β-sheet quaternary structures[29,30], we hypothesized that lining up Cys-Cys motifs in Aβ amyloid fibrils should create *in trans* FlAsH binding sites, affording conjugate fluorescence

Author Manuscript Author Manuscript Author Manuscript Author Manuscript

intensity that is proportional to the mass of fibrils being generated (Fig. 1a). Moreover, since spherical aggregate formation is also envisioned to line up some of the N-termini of Cys-Cys-Aβ, we reasoned that oligomer formation would also create *in trans* FlAsH binding sites and conjugate fluorescence proportional to the extent of oligomer formation (Fig. 1a). Since ThT binds much more strongly to fibrils than oligomers, we reasoned that we could take advantage of the spectral overlap of ThT and FlAsH to accomplish ThT-to-FlAsH FRET to differentiate fibrils from oligomers.

RESULTS

Reversible binding of FlAsH to Cys-Cys-Aβ$_{1-40}$ fibrils

Aβ$_{1-40}$ with two consecutive cysteine residues at its N-terminus (CC-Aβ$_{1-40}$) was synthesized (Fig. 1a) using an Fmoc-based solid-phase strategy. CC-Aβ$_{1-40}$ and Aβ$_{1-40}$ (10 μM) amyloidogenesis time courses are indistinguishable, demonstrating that the addition of two cysteine residues does not affect the kinetics of Aβ$_{1-40}$ aggregation, as classically monitored by ThT fluorescence (20 μM) (Fig. 1b). The identical ThT-based kinetics were expected because in published amyloid structures the N-terminal residues of Aβ$_{1-40}$ are disordered[29,30]. The fibrils resulting from CC-Aβ$_{1-40}$ and Aβ$_{1-40}$ were indistinguishable by AFM (Fig. 1b, inset) (See Supplementary Methods for the AFM method employed). Aβ was monomerized for these experiments by dissolution in 15 mM NaOH containing the reductant TCEP (3.5 mM) followed by sonication for 2 h in an ice-cold water bath before being passed through a 0.22 μm Millipore filter and then through a 10 kDa cut-off Centricon filter. FlAsH binds to CC-Aβ$_{1-40}$ amyloid fibrils, as reflected by the large increase in fluorescence intensity (Fig. 1c), however FlAsH does not bind to the CC-Aβ$_{1-40}$ monomer or Aβ$_{1-40}$ fibrils missing the N-terminal CC tag, demonstrating that FlAsH is not binding to hydrophobic patches on Aβ amyloid fibrils.

Next, we examined if FlAsH binding to amyloid is reversible–the ability to report on real-time conformational changes during Aβ aggregation would be a useful feature of this methodology. To probe reversibility, we monitored small-molecule-mediated disaggregation of existing fibrils. When FlAsH-labeled CC-Aβ$_{1-40}$ fibrils were incubated with curcumin or resveratrol, established Aβ fibril disaggregators[31,32], FlAsH binding was diminished in a dose-dependent manner (Supplementary Results, Supplementary Fig. 1). This qualitatively indicates the FlAsH binding is reversible. It is important to remember that high concentrations of the reductants ethanedithiol (1 mM) and TCEP (3.5 mM) in the disaggregation reaction are required to enable facile disulfide exchange and reversible FlAsH binding. This reversibility was envisioned to minimize the possibility that FlAsH binding to CC-Aβ$_{1-40}$ would create kinetically stable structures that do not normally exist during Aβ$_{1-40}$ aggregation. Furthermore, evidence is presented below that FlAsH binding does not noticeably alter aggregation kinetics, (also suggested by the ThT time courses in Fig. 1b). Since a high concentration of reducing reagents is required for the application of this fluorescence method, one has to be thoughtful when applying this technology to aggregation-prone proteins containing intramolecular disulfide bonds, which would likely be reduced under these conditions.

Author Manuscript Author Manuscript Author Manuscript Author Manuscript

FlAsH fluorescence detection of aggregation intermediates

Thioflavin T fluorescence did not increase until after 12 h into a $A\beta_{1-40}$ aggregation time course, at which point a rapid signal increase was observed, classically interpreted as the post-nucleation amyloid fibril "growth phase" (Fig. 1b)[16,17]. We next monitored a CC-$A\beta_{1-40}$ (10 μM) aggregation time course by FlAsH fluorescence (excitation 508 nm, emission 560 nm) using a fluorescence plate reader (shaking for 5 s every 10 min) to investigate whether FlAsH binding-associated fluorescence could be used to detect soluble CC-$A\beta_{1-40}$ oligomer formation (Fig. 1a). When initially monomeric CC-$A\beta_{1-40}$ was incubated with FlAsH (0.5 μM), a rapid increase in FlAsH–CC-$A\beta_{1-40}$ conjugate fluorescence was observed (Fig. 2a) reaching a maximum at 3 h, clearly preceding the ThT-monitored "growth phase" (cf. Fig. 2a to Fig. 1b) associated with amyloid fibril formation. FlAsH fluorescence was not observed with $A\beta_{1-40}$ lacking the N-terminal CC tag, suggesting that FlAsH does not bind non-specifically to $A\beta_{1-40}$ oligomers (light scattering data shown below demonstrate that $A\beta_{1-40}$ does form oligomers on the same time scale as CC-$A\beta_{1-40}$). Nor did FlAsH exhibit binding to $A\beta_{1-40}$ harboring a single N-terminal Cys residue (C-$A\beta_{1-40}$), implying formation of the split tetra-Cys motif is realized by misassembly-based alignment of two extended CC-$A\beta_{1-40}$ peptides (**Figs.** 1a and 2a). It is notable that a second FlAsH-based fluorescence transition is observed at t = 12 h (Fig. 2a), coincident with the ThT-monitored fibril growth phase (Fig. 1b). Addition of sonicated fibrillar $A\beta_{1-40}$ accelerated the appearance of the second FlAsH-based transition in a dose dependent manner, consistent with seeding of amyloid fibril formation (Fig. 2b)[16]. That this dip and then increase in FlAsH fluorescence (Fig. 2b) correlates with the dose-dependent shortening of the lag phase in a ThT-monitored aggregation reaction by seeding (cf. **Fig. 2b** to **2c**) suggests that this transition reports on Aβ fibril formation.

To see if FlAsH binding influences $A\beta_{1-40}$ aggregation kinetics, CC-$A\beta_{1-40}$ aggregation time courses were monitored by ThT fluorescence in the presence or absence of FlAsH. As shown in Figure 2d, the "amyloid growth phase" t_{50}'s are within error, evidence that FlAsH binding does not noticeably alter $A\beta_{1-40}$ oligomerization or fibrillization equilibria. Notably, the ThT amplitude in the presence of FlAsH is much lower than in its absence, due to non-radiative energy transfer from ThT to FlAsH. When FlAsH-labeled CC-$A\beta_{1-40}$ fibrils were incubated with ThT and excited at 430 nm, the expected ThT emission maximum at 485 nm was observed with markedly reduced intensity, because there was a strong FlAsH emission at 530 nm (Fig. 2e), consistent with ThT to FlAsH fluorescence resonance energy transfer (FRET). The emission spectra of ThT and the excitation spectra of FlAsH, exhibit overlap (Supplementary Fig. 2), consistent with the observed FRET efficiency (E) of 0.66 (Fig. 2e). Excitation of FlAsH-labeled CC-$A\beta_{1-40}$ fibrils in the absence of ThT at 430 nm afforded negligible emission (Fig. 2e) and $A\beta_{1-40}$ fibrils (not bearing a Cys-Cys tag) excited at 430 nm, to which FlAsH and ThT were added, exhibited the expected ThT emission at 485 nm (Fig. 2e), supporting the hypothesis ThT and FlAsH need to be proximally bound for non-radiative transfer of ThT excited state energy to FlAsH to be observed.

Not all of the ThT excited state energy was transferred to FlAsH, suggesting the possibility that aggregation time courses could be monitored by both ThT and ThT-to-FlAsH FRET simultaneously. Therefore, we monitored a CC-$A\beta_{1-40}$ aggregation time course with both

Author Manuscript Author Manuscript Author Manuscript Author Manuscript

FlAsH (0.5 μM) and ThT (20 μM) utilizing FlAsH fluorescence, ThT fluorescence, and ThT-to-FlAsH FRET, employing three different excitation / emission wavelengths to maximize each. As shown in Fig. 2f, both the FlAsH and ThT-based fluorescence time-courses were those expected from the data presented above (cf. to Fig. 2a and Fig. 2d, respectively). Moreover, FRET from ThT-to-FlAsH was observed in the CC-Aβ_{1-40} aggregation time course (Fig. 2f). The early low amplitude FRET reflects the fact that some ThT is bound coincident with FlAsH on oligomers (weak ThT binding to oligomers was previously reported[21,33]), whereas the intense FRET transition reflects the nucleated conformational conversion of oligomers into fibrils.

Further evidence for nucleated conformational conversion

All of our observations regarding the aggregation of CC-Aβ_{1-40} utilizing FlAsH, ThT and ThT-to-FlAsH FRET suggest that Aβ aggregates very rapidly into oligomers, which slowly convert into fibrils. Prior experimental determinations utilizing surface tension measurements and pyrene fluorescence to measure the Aβ oligomer critical micelle concentration[14], as well as temporal quasielastic light scattering measurements on Aβ aggregation time courses[13] also strongly support this hypothesis. These data suggest that Aβ aggregates by a mechanism akin to the nucleated conformational conversion mechanism first proposed by Lindquist et al.[34] to explain the fast forming Sup35 oligomers that slowly convert into amyloid fibrils. Such a mechanism has also been proposed for human amyloidogenic peptides such as huntingtin and islet amyloid polypeptide[35,36]. In this mechanism, the rate limiting step (conversion of oligomers to fibrils) is accelerated by adding fibrillar seeds (shown in Fig. 2b herein in the case of Aβ).

To provide further evidence for the rapid formation of Aβ_{1-40} oligomers, dynamic light scattering time courses were recorded (Fig. 3a). Initially monomeric CC-Aβ_{1-40} (10 μM) or Aβ_{1-40} (10 μM) in a scintillation vial was incubated for 5 h at 37 °C and light scattering at 90° was recorded every 4 sec. During the incubation, the vial was taken out every 10 min for vortex-based shaking for 5 sec. Note that the shaking condition is distinct from that used by the plate reader. The dynamic light scattering time courses for Aβ_{1-40}, CC-Aβ_{1-40}, and CC-Aβ_{1-40} + FlAsH were similar, reaching plateaus around 0.18 (arbitrary units) within 5 h. Because of the agitation conditions used, sample to sample variations are generally larger than the differences in the time courses shown in Fig. 3a, thus the observed differences are not considered to be significant. Notably, both Aβ_{1-40} and CC-Aβ_{1-40} displayed a rapid increase in light scattering that plateaus before the commencement of the ThT-detected “growth phase”, providing strong independent evidence for the rapid formation of soluble oligomers preceding slow fibril formation. Structural conversion of Aβ oligomers to fibrils exhibiting a β-sheet structure has also been observed by NMR spectroscopy[37,38], further supporting our observations. That the dynamic light scattering time courses of CC-Aβ_{1-40} vs. CC-Aβ_{1-40} + FlAsH were similar (Fig. 3a), provide additional support (beyond the ThT data outlined in Fig. 2d and discussed above) for the hypothesis that FlAsH binding does not significantly perturb the oligomerization and fibrillization equilibria that are likely linked.

Aβ_{1-40} aggregation was also monitored using the A11 antibody, which selectively recognizes soluble oligomers of Aβ over monomers and Aβ fibrils. A11 also selectively

Author Manuscript Author Manuscript Author Manuscript Author Manuscript

recognizes oligomers of other peptides or proteins such as α-synuclein, human insulin, polyglutamine, lysozyme, and prion[22]. As shown in Fig. 3b, A11-immunoreactive oligomers show up early (3 and 5 h) in the CC-$A\beta_{1-40}$ aggregation time course and then disappear after the oligomers convert to fibrils (21 h). The 6E10 anti-Aβ antibody, which detects all forms of Aβ by recognizing an epitope which lies within amino acids 3-8 (EFRHDS), was used to demonstrate that similar amounts of Aβ were present in all samples (See Supplementary Methods for the dot blot methodology used).

Since the lack of Aβ oligomer quantification in the past has allowed those that favor the nucleated polymerization mechanism to dismiss oligomers as a minor unimportant population, we quantified the amount of CC-$A\beta_{1-40}$ oligomers (Fig. 3c). A membrane with a molecular weight cut-off of 50 kDa was used to filter CC-$A\beta_{1-40}$ as a function of time in the aggregation time course. The CC-$A\beta_{1-40}$ passing through the membrane was quantified employing a Bradford assay. The amount of CC-$A\beta_{1-40}$ passing through the filter decreases rapidly over time, reaching a plateau after 3 h at which time ~85% of CC-$A\beta_{1-40}$ forms oligomers retained by the filter. This strongly supports the hypothesis that the early increase in CC-$A\beta_{1-40}$ FlAsH fluorescence reflects soluble oligomer formation exhibiting a high chemical yield (85%), while the second transition (decrease followed by an increase in FlAsH fluorescence) reflects a nucleated conformational conversion of Aβ oligomers into fibrils (Fig. 2a).

AFM images reveal spherical species increasing in concentration early in the CC-$A\beta_{1-40}$ aggregation time course (Fig. 3d). The soluble oligomers formed 3 h into the time course were 3-4 nm in height, which is in accordance with previous reports on the height of spherical aggregates[38]. Directly following the second FlAsH transition (i.e., after the ThT detected “amyloid growth phase”, t = 13h), we observe that CC-$A\beta_{1-40}$ now has a fibrillar morphology by AFM (Fig. 3d). Notably, these images show what appears to be spherical aggregates adding to the end of each fibril (see the inset of Fig. 3d), suggesting that the aggregates are on pathway for fibril formation. Alignments of multiple end segments with an average height of 3-4 nm were observed, consistent with the height of soluble oligomers. Addition of soluble oligomers to the ends of fibrils is strictly analogous to what the Lindquist group observed for the Sup35 nucleated conformational conversion[34].

It is critical to demonstrate that the $A\beta_{1-40}$ oligomers are kinetically competent to form amyloid fibrils, and are thus on-pathway intermediates. In other words, oligomers should form fibrils faster than $A\beta_{1-40}$ monomers do. Monomeric $A\beta_{1-40}$ was incubated for 3.5 h during which time an 85% yield of oligomers form (**Figs 3a** and **c**). The oligomers were either studied directly or diluted with variable amounts of freshly monomerized $A\beta_{1-40}$ and then their fibril formation kinetics were monitored by ThT fluorescence. As show in Fig. 3e, the rate of fibril formation was dependent on the amount of the oligomers present at the beginning of reaction, the more oligomers the faster the conversion to fibrils, demonstrating the kinetic competence of oligomers for fibril formation. Moreover, the higher the proportion of oligomers, the greater the susceptibility to seeding amyloid fibril formation by preformed seeds (Fig. 3e). Taken together, the determination that oligomers represent the vast majority of $A\beta_{1-40}$ species present after 2 h and that they are kinetically competent to form amyloid fibrils *in vitro* provides compelling evidence in favor of a nucleated

Author Manuscript Author Manuscript Author Manuscript Author Manuscript

conformational conversion mechanism of $A\beta_{1-40}$ amyloidogenesis. This, in combination with the remainder of the above presented data, and additional compelling data from other laboratories very strongly support abandoning the nucleated polymerization mechanism of $A\beta_{1-40}$ amyloidogenesis in favor of a nucleated conformational conversion mechanism.

Aggregation Properties of AD-associated Aβ mutants

Early-onset AD is associated with several mutations in Aβ that typically cause subtle changes in the mechanism of Aβ aggregation. These mechanistic changes are difficult to assess by traditional methods, but the split-FlAsH aggregation sensor is ideal for characterizing such changes. We illustrate this point with two familial AD examples.

One such mutation is the Aβ E22G mutation (E693G in APP), also known as the arctic mutation, that is reported to have enhanced protofibril formation and enhanced proteotoxicity[39,40]. CC-E22G-$A\beta_{1-40}$ exhibited a 2-fold faster conversion of soluble oligomers to cross-β-sheet structures relative to WT, apparently through nucleated conformational conversion (cf. Fig. 4a to Fig. 2f). AFM analysis of CC-E22G-$A\beta_{1-40}$ 24 h into the aggregation time course shows morphology similar to that previously reported for protofibrils of $A\beta_{1-40}$[40] (Fig. 4b, left panel).

We also examined the familial Alzheimer's E22 deletion mutant (Aβ E22Δ), which is reported to exclusively form soluble oligomers that very slowly convert to fibrils, if at all[41], leading to more potent synaptic alterations than WT Aβ. No plaque formation was observed in the post-mortem brains of aged mice harboring this AD mutation[15]. CC-E22Δ-$A\beta_{1-40}$ exhibited a fast increase in FlAsH fluorescence with an intensity 1.5 fold greater than that of CC-$A\beta_{1-40}$, indicating the formation of more soluble oligomers (Fig. 4c). Notably, a second FlAsH fluorescence transition reflecting nucleated conformational conversion to fibrils was not observed with E22Δ within 24 h (Fig. 4c). Nor did ThT fluorescence increase, again indicating no fibril formation over a 24 h time course. A dot-blot assay showed the presence of sustained oligomer formation 24 h into the aggregation time course only with CC-E22Δ-$A\beta_{1-40}$ (Fig. 4d). AFM analysis also confirmed the presence of spherical oligomers at 24 h (Fig. 4b, right panel). This variant of $A\beta_{1-40}$ that undergoes sustained oligomer formation should be a very useful research tool.

Understanding how lipids influence Aβ aggregation

Aβ aggregation is known to be modulated by lipids. Recent lipidomics studies suggest that altered lipid compositions in neuronal cell membranes correlate strongly with the onset and severity of AD[42,43]. For example, significantly higher levels of serine phospholipids, such as POPS (1-palmitoyl-2-oleoyl-*sn*-glycero-3-phospho-L-serine), were found in AD patient brains compared to age-matched control brains, implying that the POPS concentration could be used as a biomarker for detecting AD[42]. In contrast, significant decreases of plasmalogen ethanolamine (PlsEtn) were observed in AD patients vs. age-matched controls, also having appeal as a biomarker for early AD diagnosis[44]. In fact, the extent of the decrease of PlsEtn correlated well with the severity of AD[43]. Notably, PlsEtn constitutes 30 mol % of total phospholipids and 90 mol % of the ethanolamine phospholipids in neuronal cell membranes[44].

Author Manuscript Author Manuscript Author Manuscript Author Manuscript

However, it is not yet clear from a mechanistic perspective how lipids influence the progress of AD. Recent studies have started to provide evidence that lipids may strongly influence Aβ aggregation and proteotoxicity[45]. In most of the published studies, aggregation as a function of lipid composition was followed using ThT fluorescence, which was shown herein to monitor only fibril formation (insensitive to oligomer formation). We illustrate here that the split-FlAsH aggregation sensor represents a powerful methodology for determining how lipids influence Aβ aggregation. All lipids used in these studies (Fig. 5a) were employed as large unilamellar vesicles (LUVs), exhibiting an average size of 100 nm in diameter, as characterized by light scattering analysis (Supplementary Fig. 3).

Initially monomeric CC-Aβ_{1-40} was incubated with lipid vesicles in a 1:8 molar ratio (by monomer concentration) and aggregation was monitored by FlAsH fluorescence, ThT fluorescence, and ThT-to-FlAsH FRET (Fig. 5b and Supplementary Fig. 4). CC-Aβ_{1-40} incubated with POPS LUVs exhibited rates of oligomer formation similar to those of CC-Aβ_{1-40} in the absence of LUVs. However, POPS LUVs notably delayed nucleated conformational conversion of CC-Aβ_{1-40} to amyloid fibrils relative to CC-Aβ_{1-40} in the absence of LUVs (Fig. 5b). In contrast, POPC (1-palmitoyl-2-oleoyl-*sn*-glycero-3-phosphocholine) LUVs, comprising a neutral, zwitterionic head group, exhibited a more rapid nucleated conformational conversion of CC-Aβ_{1-40} to amyloid fibrils (Fig. 5b).

Most significantly, CC-Aβ_{1-40} incubated with PlsEtn LUVs did not exhibit the rapid FlAsH fluorescence associated with CC-Aβ_{1-40} oligomer formation (Fig. 5b). However, PlsEtn LUVs still enabled sluggish fibril formation (Fig. 5b). The PlsEtn we used was 1-(1*Z*-octadecenyl)-2-arachidonoyl-*sn*-glycero-3-phosphoethanolamine, because its deficiency in AD has been reported[43] and owing to its commercially availability. A dot-blot assay employing the A11 antibody confirmed the inhibition of oligomer formation with PlsEtn LUVs (Fig. 5c). Fibril morphology was observed at 18 h from CC-Aβ_{1-40} incubated with PlsEtn (Fig. 5d, left panel). In contrast, CC-Aβ_{1-40} incubated with POPS LUVs showed sustained spherical oligomers at 18 h (Fig. 5d, right panel). When CC-Aβ_{1-40} fibrils were added to the CC-Aβ_{1-40} + PlsEtn LUV solution at t = 90 min, a rapid increase of FlAsH fluorescence was observed (Supplementary Fig. 5). This control experiment rules out the possibility that the absence of an early FlAsH fluorescence increase with PlsEtn is due to the encapsulation of FlAsH in PlsEtn vesicles.

DISCUSSION

The characterization of protein aggregation mechanisms is limited by the tools that we have and the corresponding observations we can make—detecting and quantifying small oligomers is especially challenging. Currently, establishing the sequence of events in a protein aggregation reaction requires the laborious application of many experimental approaches, not all of which are available to many laboratories, like dynamic light scattering experiments. Herein, we have shown that split-FlAsH aggregation sensors can greatly simplify mechanistic studies on protein aggregation by providing much more information than ThT monitoring alone. Because split-FlAsH aggregation sensors can differentially detect both oligomers and fibrils when used in combination with ThT fluorescence monitoring of fibrillization, parallel monitoring of the fluorescence signal from FlAsH, the

Author Manuscript Author Manuscript Author Manuscript Author Manuscript

fluorescence signal from ThT, and the FRET signal between ThT and FlAsH readily reveals the details of the Aβ aggregation mechanism *in vitro*. Our data compels us to abandon the description of Aβ aggregation as a nucleated polymerization; Aβ aggregation is more consistent with a nucleated conformational conversion (Fig. 6). This hypothesis is validated by several lines of evidence in this work and that of others[13,14]. From a practical perspective, it is important to note that the split FlAsH aggregation assays shown in **Figs.** 2, 4 and 5 were carried out in a fluorescence plate reader, available to nearly all researchers.

The split-FlAsH aggregation sensor reported herein is not the first fluorescence-based aggregation sensor. Kim and co-workers created aggregation sensors by covalently attaching green fluorescent protein (GFP) to the aggregation-prone protein of interest[46]. The observation of fluorescent puncta that do not exhibit rapid recovery from photobleaching are defined as aggregates *in vitro* and *in vivo*. Outeiro and co-workers have reported a split-GFP aggregation sensor for α-synuclein[47]; Yushchenko and co-workers used an environment sensitive fluorophore (3-hydroxychormone) to label an Ala-to-Cys mutant of α-synuclein to report on misassembly[48]; and Roberti and co-workers have used FlAsH binding to a tetracysteine FlAsH binding site to monitor α-synuclein aggregation[49].

Our split FlAsH method combines the best features of these prior approaches. The short tag and the small molecule employed as the fluorophore minimizes the perturbation to the aggregation mechanism. Our use of a split-FlAsH sensor minimizes the background fluorescence, ensuring that the observation of FlAsH fluorescence is conditional on aggregation. However, the requirement for reductants to achieve FlAsH binding reversibility and to ensure that the Cys-Cys motif does not form unwanted disulfides needs to be considered when applying this methodology to aggregation-prone proteins harboring disulfide bonds.

The utilization of split-FlAsH aggregation sensors with other non-disulfide containing aggregation-prone proteins should be a straightforward extension of the method presented here. We envision that recording the fluorescence from the split-FlAsH aggregation sensor directly along with parallel monitoring of ThT fluorescence and ThT-to-FlAsH FRET should suffice to rapidly and definitively characterize the key features of the aggregation mechanism of most proteins. Simply adding Cys-Cys to one of the termini or mutating two sequential residues to Cys in a part of an aggregation-prone protein of interest that does not comprise the fibril core creates the split-FlAsH binding site. After validating that FlAsH does not bind to the monomerized protein or the protein in its native quaternary structure and that the two Cys residues do not disrupt the aggregation mechanism based on ThT fluorescence, the protein is ready for *in vitro*, and in principle, *in vivo* mechanistic studies. Oligomer structures are broadly similar from protein to protein, as evidenced by the ability of the A11 antibody to recognize oligomers derived from many different proteins, hence this approach should be generally applicable[22]. Fibril structures are also similar for different proteins, as evidenced by historic fibril diffraction studies and current solid state NMR experiments[50]. Thus, we expect split-FlAsH aggregation sensors in other proteins to behave much like the one in Aβ, with both oligomers and fibrils being detectable and distinguishable.

Author Manuscript Author Manuscript Author Manuscript Author Manuscript

In summary, a FlAsH-based aggregation sensor is presented that can detect and differentiate oligomers (FlAsH fluorescence, low-efficiency ThT-to-FlAsH FRET) from amyloid fibrils (FlAsH fluorescence, ThT fluorescence, high-efficiency ThT-to-FlAsH FRET) in time course studies carried out in a fluorescence plate reader *in vitro*. The totality of the data presented reinforce other previously published observations that Aβ aggregates by a nucleated conformational conversion mechanism (Fig. 6). Notably, the split-FlAsH aggregation sensor sensitively revealed the differential effects of Aβ mutations and lipid vesicles on the Aβ aggregation process. Because the termini of many amyloid fibrils are disordered, we envision that adding Cys-Cys to a variety of aggregation-prone proteins will easily allow investigators to differentiate oligomer formation from fibril formation in a convenient fluorescence plate reader format using FlAsH.

METHODS

Preparation of monomers and fibrils of Aβ

Synthetic Aβ and its variants with following sequences were prepared on an ABI 433A solid phase peptide synthesizer (Applied Biosystems) employing an Fmoc-chemistry strategy: DAEFRHDSGYEVHHQKLVFFAEDVGSNKGA IIGLMVGGVV ($Aβ_{1-40}$), CDAEFRHDSGYEVHHQKLVFFAEDVGSNKGAIIGLMVGGVV (C-$Aβ_{1-40}$), CCDAEFRHDSGYEVHHQKLVFFAEDVGSNKGAIIGLMVGGVV (CC-$Aβ_{1-40}$), CCDAEFRHDSGYEVHHQKLVFFAGDVGSNKGAIIGLMVGGVV (CC-$Aβ_{1-40}$E22G), CCDAEFRHDSGYEVHHQKLVFFA_DVGSNKGAIIGLMVGGVV (CC-$Aβ_{1-40}$E22Δ). The Aβ peptides were dissolved in 1,1,1,3,3,3-hexafluoro-2-propanol (HFIP, Sigma) and incubated at 25 °C for 2 h. HFIP was removed by blowing a gentle stream of Ar over the solution and the resulting film of peptide was stored at −20 °C before use. Monomerization of Aβ continued by dissolving peptides in 15 mM NaOH (350 μL) with 3.5 mM tris(2-carboxyethyl)phosphine (TCEP, Thermo Scientific) added followed by sonication for 2 h in ice-cold water bath. The resulting solution was then first passed through a 0.22 μm filter (Millipore) followed by passage through a 10 kDa cut-off Centricon filter (Millipore). Monomerized Aβ was kept on ice and used within 3h. For the preparative formation of fibrils, the monomerized $Aβ_{1-40}$ solution was diluted with 50 mM sodium phosphate buffer (300 mM NaCl, 3.5 mM TCEP, pH 7.4) to a concentration of 10 μM and incubated for 5-7 days at 37 °C with constant rotation (24 rpm) on a EchoTherm™ RT11 Rotating Mixer (Torrey Pines Scientific Inc.). For seeding experiments, the resulting fibrils were bath-sonicated for 20 min in ice-cold water bath before use.

ThT and FlAsH binding Aβ as a function of quaternary structure

To assess ThT binding, a solution containing monomeric (10 μM) or fibrillar (43.3 μg / mL) $Aβ_{1-40}$ in the aggregation buffer (50 mM Na phosphate, 300 mM NaCl, 1 mM EDTA, 1 mM 1,2 ethanedithiol (EDT), pH 7.4) was incubated with ThT (20 μM) for 1 min at room temperature. The ThT emission fluorescence (460 nm – 550 nm) was measured using a fluorescence spectrometer (CARY Eclipse, VARIAN) with excitation wavelength of 430 nm. To evaulate FlAsH binding of monomeric $Aβ_{1-40}$, the solution containing $Aβ_{1-40}$ (10 μM) in the aggregation buffer was incubated with FlAsH (100 μM, Invitrogen) for 1 h at room temperature. The solution was passed through a gel-filtration column (Sephadex G-25

Author Manuscript Author Manuscript Author Manuscript Author Manuscript

fine, Amersham Bioscience) to remove unbound FlAsH dye and the fractions containing Aβ were pooled and used for fluorescence measurement. The emission of FlAsH (515 – 650 nm) was evaluated employing an excitation wavelength of 508 nm. To ascertain the FlAsH binding of the fibrils, they were treated with FlAsH(100 μM) and unbound FlAsH was removed by centrifugation (12,000 g) and the fluorescence was measured as described above.

Disaggregation assay with curcumin and resveratrol

A FlAsH CC-Aβ_{1-40} fibril complex (prepared as described above) was incubated in the aggregation buffer as a function of curcumin or resveratrol concentration at 37 °C. After 12 h incubation, the FlAsH fluorescence was measured as described above.

Monitoring aggregation of Aβ by ThT, FlAsH, and ThT-to-FlAsH FRET

Mono merized Aβ_{1-40} or its variants were incubated in the aggregation buffer with ThT (20 μM), or FlAsH (500 nM), or both FlAsH and ThT (37 °C) in a plate reader (Spectramax Gemini EM fluorescence plate reader, Molecular Devices). The fluorescence was measured every 10 min after shaking for 5 sec with the following excitation and emission wavelength settings: ThT (Ex. 430, Em. 485), FlAsH (Ex. 508, Em. 560), ThT-to-FlAsH FRET (Ex. 430, Em. 560). To examine whether oligomers are kinetically competent to form fibrils, fibrillization was monitored by ThT fluorescence as following. Freshly monomerized Aβ_{1-40} (10 μM) in the aggregation buffer in a 96-well plate was incubated (37 °C) in a plate reader for 3.5 h with shaking for 5 sec every 10 min to form oligomers. The plate was removed from the plate reader and kept at room temperature for 30 min. Then, the oligomers were mixed with variable amounts of freshly monomerized Aβ_{1-40} and seeds (0.5%). ThT (20 μM) was added to samples and ThT fluorescence was measured as described above.

Dynamic light scattering

Aggregation buffer was filtered through a 0.22 μm filter (Millipore) into a scintillation vial. Scattered laser light intensities measured at a 90° angle were monitored over time (about 1 h) at 37 °C with a Dawn EOS light scattering photometer (Wyatt Technology) until no increase in the scattered intensity was observed. Monomerized Aβ_{1-40} was added and scattered laser light intensities measured at a 90° angle were recorded every 4 sec for 5 h. During the time course, the vial was taken out every 10 min for vortex shaking (Fisher Vortex Genie 2, Fisher Scientific) for 5 sec.

Quantitation of oligomer formation

Freshly monomerized CC-Aβ_{1-40} (10 μM) was incubated in the aggregation buffer (final volume = 100 μL) at 37 °C in a plate reader with shaking for 5 sec every 10 min. At the indicated time points, to measure the amount of total CC-Aβ_{1-40} , 20 μL of the aggregation reaction solution was mixed with 80 μL of Coomassie PlusTM Protein Assay Reagent (THERMO Scientific) and absorbance at 595 nm was measured (Bradford assay). The remaining 80 μL of the reaction solution was loaded onto a Ultracel YM-50 filter (Millipore, 50 kDa molecular weight cut-off) and was centrifuged at 14,000 rpm at 4°C for 20 min. The

Author Manuscript Author Manuscript Author Manuscript Author Manuscript

protein concentration in 20 μL of the filtrate was measured in the Bradford assay as described above.

Preparation of lipid LUVs

Lipid (0.6 mg, Avanti Polar Lipids) was dissolved in 500 μL of $CHCl_3$. The solvent was removed by blowing a gentle stream of Ar over the solution and the lipid sample was dried *in vacuo* for 1 h. The residual lipid film was hydrated with 480 μL aggregation buffer at 25 °C for 1 h. After vortexing, the solution was sonicated using a bath sonicator (Laboratory Supplies Company Inc.) for 3 – 20 min at 20 °C until a clear solution was obtained. The size of lipid vesicle was determined by static light scattering using a Dawn EOS light scattering photometer. To study the effect of lipids on $A\beta_{1\text{-}40}$ aggregation, lipid LUVs (80 μM monomer concentration) were included in the aggregation reaction.

Supplementary Material

Refer to Web version on PubMed Central for supplementary material.

ACKNOWLEDGEMENTS

We thank NIH (NS050636), The Skaggs Institute for Chemical Biology, and the Lita Annenberg Hazen Foundation for financial support and Dr. Colleen Fearns for critical feedback on the manuscript.

REFERENCES

1. Selkoe DJ. The molecular pathology of Alzheimer’s disease. Neuron. 1991; 6:487–498. [PubMed: 1673054]
2. Hardy J. The Alzheimer family of diseases: many etiologies, one pathogenesis? Proc Natl Acad Sci U S A. 1997; 94:2095–2097. [PubMed: 9122152]
3. Holtzman DM, Morris JC, Goate AM. Alzheimer’s disease: the challenge of the second century. Sci Transl Med. 2011; 3:77sr71.
4. Klein WL, Krafft GA, Finch CE. Targeting small Abeta oligomers: the solution to an Alzheimer’s disease conundrum? Trends Neurosci. 2001; 24:219–224. [PubMed: 11250006]
5. Walsh DM, Selkoe DJ. A beta oligomers - a decade of discovery. J Neurochem. 2007; 101:1172–1184. [PubMed: 17286590]
6. Shankar GM, et al. Amyloid-beta protein dimers isolated directly from Alzheimer’s brains impair synaptic plasticity and memory. Nat Med. 2008; 14:837–842. [PubMed: 18568035]
7. Shoji M, et al. Production of the Alzheimer amyloid beta protein by normal proteolytic processing. Science. 1992; 258:126–129. [PubMed: 1439760]
8. Garzon-Rodriguez W, Sepulveda-Becerra M, Milton S, Glabe CG. Soluble amyloid Abeta-(1-40) exists as a stable dimer at low concentrations. J Biol Chem. 1997; 272:21037–21044. [PubMed: 9261105]
9. Ono K, Condron MM, Teplow DB. Structure-neurotoxicity relationships of amyloid beta-protein oligomers. Proc Natl Acad Sci U S A. 2009; 106:14745–14750. [PubMed: 19706468]
10. Bernstein SL, et al. Amyloid-beta protein oligomerization and the importance of tetramers and dodecamers in the aetiology of Alzheimer’s disease. Nat Chem. 2009; 1:326–331. [PubMed: 20703363]
11. Lesne S, et al. A specific amyloid-beta protein assembly in the brain impairs memory. Nature. 2006; 440:352–357. [PubMed: 16541076]
12. Lambert MP, et al. Diffusible, nonfibrillar ligands derived from Abeta1-42 are potent central nervous system neurotoxins. Proc Natl Acad Sci U S A. 1998; 95:6448–6453. [PubMed: 9600986]

Author Manuscript Author Manuscript Author Manuscript Author Manuscript

13. Lomakin A, Teplow DB, Kirschner DA, Benedek GB. Kinetic theory of fibrillogenesis of amyloid-beta protein. Proc. Natl. Acad. Sci. U. S. A. 1997; 94:7942–7947. [PubMed: 9223292]
14. Sabate R, Estelrich J. Evidence of the existence of micelles in the fibrillogenesis of beta-amyloid peptide. J Phys Chem B. 2005; 109:11027–11032. [PubMed: 16852343]
15. Tomiyama T, et al. A mouse model of amyloid beta oligomers: their contribution to synaptic alteration, abnormal tau phosphorylation, glial activation, and neuronal loss in vivo. J Neurosci. 2010; 30:4845–4856. [PubMed: 20371804]
16. Harper JD, Lansbury PT Jr. Models of amyloid seeding in Alzheimer's disease and scrapie: mechanistic truths and physiological consequences of the time-dependent solubility of amyloid proteins. Annu Rev Biochem. 1997; 66:385–407. [PubMed: 9242912]
17. Jarrett JT, Lansbury PT Jr. Seeding "one-dimensional crystallization" of amyloid: A pathogenic mechanism in Alzheimer's disease and scrapie? Cell. 1993; 73:1055–1058. [PubMed: 8513491]
18. Roychaudhuri R, Yang M, Hoshi MM, Teplow DB. Amyloid beta-protein assembly and Alzheimer disease. J Biol Chem. 2009; 284:4749–4753. [PubMed: 18845536]
19. Wetzel R. Kinetics and thermodynamics of amyloid fibril assembly. Acc Chem Res. 2006; 39:671–679. [PubMed: 16981684]
20. LeVine H 3rd. Thioflavine T interaction with synthetic Alzheimer's disease beta-amyloid peptides: detection of amyloid aggregation in solution. Protein Sci. 1993; 2:404–410. [PubMed: 8453378]
21. Bieschke J, Zhang Q, Powers ET, Lerner RA, Kelly JW. Oxidative Metabolites Accelerate Alzheimer's Amyloidogenesis by a Two-Step Mechanism, Eliminating the Requirement for Nucleation. Biochemistry. 2005; 44:4977–4983. [PubMed: 15794636]
22. Kayed R, et al. Common structure of soluble amyloid oligomers implies common mechanism of pathogenesis. Science. 2003; 300:486–489. [PubMed: 12702875]
23. Griffin BA, Adams SR, Tsien RY. Specific covalent labeling of recombinant protein molecules inside live cells. Science. 1998; 281:269–272. [PubMed: 9657724]
24. Coleman BM, et al. Conformational detection of prion protein with biarsenical labeling and FlAsH fluorescence. Biochem Biophys Res Commun. 2009; 380:564–568. [PubMed: 19285001]
25. Luedtke NW, Dexter RJ, Fried DB, Schepartz A. Surveying polypeptide and protein domain conformation and association with FlAsH and ReAsH. Nat Chem Biol. 2007; 3:779–784. [PubMed: 17982447]
26. Krishnan B, Gierasch LM. Cross-strand split tetra-Cys motifs as structure sensors in a beta-sheet protein. Chem Biol. 2008; 15:1104–1115. [PubMed: 18940670]
27. Goodman JL, Fried DB, Schepartz A. Bipartite tetracysteine display requires site flexibility for ReAsH coordination. Chembiochem. 2009; 10:1644–1647. [PubMed: 19533719]
28. Webber TM, et al. Conformational detection of p53's oligomeric state by FlAsH Fluorescence. Biochem Biophys Res Commun. 2009; 384:66–70. [PubMed: 19393630]
29. Petkova AT, et al. A structural model for Alzheimer's beta -amyloid fibrils based on experimental constraints from solid state NMR. Proc Natl Acad Sci U S A. 2002; 99:16742–16747. [PubMed: 12481027]
30. Luhrs T, et al. 3D structure of Alzheimer's amyloid-beta(1-42) fibrils. Proc Natl Acad Sci U S A. 2005; 102:17342–17347. [PubMed: 16293696]
31. Porat Y, Abramowitz A, Gazit E. Inhibition of amyloid fibril formation by polyphenols: structural similarity and aromatic interactions as a common inhibition mechanism. Chem Biol Drug Des. 2006; 67:27–37. [PubMed: 16492146]
32. Yang F, et al. Curcumin inhibits formation of amyloid beta oligomers and fibrils, binds plaques, and reduces amyloid in vivo. J Biol Chem. 2005; 280:5892–5901. [PubMed: 15590663]
33. Maezawa I, et al. Congo red and thioflavin-T analogs detect Abeta oligomers. J Neurochem. 2008; 104:457–468. [PubMed: 17953662]
34. Serio TR, et al. Nucleated conformational conversion and the replication of conformational information by a prion determinant. Science. 2000; 289:1317–1321. [PubMed: 10958771]
35. Thakur AK, et al. Polyglutamine disruption of the huntingtin exon 1 N terminus triggers a complex aggregation mechanism. Nat Struct Mol Biol. 2009; 16:380–389. [PubMed: 19270701]

Author Manuscript Author Manuscript Author Manuscript Author Manuscript

36. Wei L, et al. The molecular basis of distinct aggregation pathways of islet amyloid polypeptide. J Biol Chem. 2011; 286:6291–6300. [PubMed: 21148563]
37. Chimon S, et al. Evidence of fibril-like beta-sheet structures in a neurotoxic amyloid intermediate of Alzheimer's beta-amyloid. Nat Struct Mol Biol. 2007
38. Ahmed M, et al. Structural conversion of neurotoxic amyloid-beta(1-42) oligomers to fibrils. Nat Struct Mol Biol. 2010; 17:561–567. [PubMed: 20383142]
39. Nilsberth C, et al. The 'Arctic' APP mutation (E693G) causes Alzheimer's disease by enhanced Abeta protofibril formation. Nat Neurosci. 2001; 4:887–893. [PubMed: 11528419]
40. Lashuel HA, et al. Mixtures of wild-type and a pathogenic (E22G) form of Abeta40 in vitro accumulate protofibrils, including amyloid pores. J Mol Biol. 2003; 332:795–808. [PubMed: 12972252]
41. Tomiyama T, et al. A new amyloid beta variant favoring oligomerization in Alzheimer's-type dementia. Ann Neurol. 2008; 63:377–387. [PubMed: 18300294]
42. Wells K, Farooqui AA, Liss L, Horrocks LA. Neural membrane phospholipids in Alzheimer disease. Neurochem Res. 1995; 20:1329–1333. [PubMed: 8786819]
43. Goodenowe DB, et al. Peripheral ethanolamine plasmalogen deficiency: a logical causative factor in Alzheimer's disease and dementia. J Lipid Res. 2007; 48:2485–2498. [PubMed: 17664527]
44. Han X, Holtzman DM, McKeel DW Jr. Plasmalogen deficiency in early Alzheimer's disease subjects and in animal models: molecular characterization using electrospray ionization mass spectrometry. J Neurochem. 2001; 77:1168–1180. [PubMed: 11359882]
45. Martins IC, et al. Lipids revert inert Abeta amyloid fibrils to neurotoxic protofibrils that affect learning in mice. EMBO J. 2008; 27:224–233. [PubMed: 18059472]
46. Kim S, Nollen EA, Kitagawa K, Bindokas VP, Morimoto RI. Polyglutamine protein aggregates are dynamic. Nat Cell Biol. 2002; 4:826–831. [PubMed: 12360295]
47. Outeiro TF, et al. Formation of toxic oligomeric alpha-synuclein species in living cells. PLoS One. 2008; 3:e1867. [PubMed: 18382657]
48. Yushchenko DA, Fauerbach JA, Thirunavukkuarasu S, Jares-Erijman EA, Jovin TM. Fluorescent ratiometric MFC probe sensitive to early stages of alpha-synuclein aggregation. J Am Chem Soc. 2010; 132:7860–7861. [PubMed: 20491471]
49. Roberti MJ, Bertoncini CW, Klement R, Jares-Erijman EA, Jovin TM. Fluorescence imaging of amyloid formation in living cells by a functional, tetracysteine-tagged alpha-synuclein. Nat Methods. 2007; 4:345–351. [PubMed: 17351621]
50. Sunde M, Blake C. The structure of amyloid fibrils by electron microscopy and X-ray diffraction. Adv Protein Chem. 1997; 50:123–159. [PubMed: 9338080]

Author Manuscript Author Manuscript Author Manuscript Author Manuscript

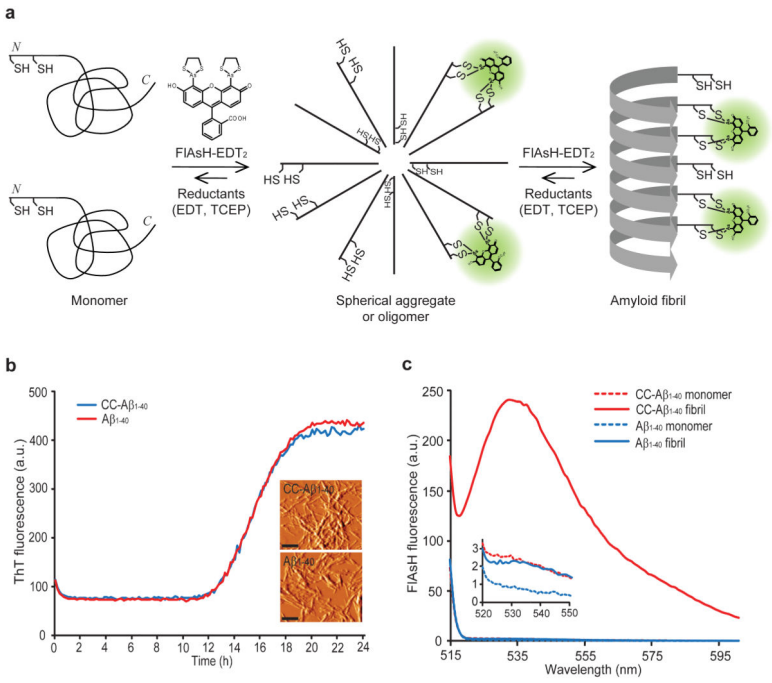

Figure 1.

Detection of Cys-Cys-A$\beta_{1\text{-}40}$ fibrils using FlAsH-EDT$_2$. (**a**) A model wherein A$\beta_{1\text{-}40}$ with two consecutive cysteines at its N terminus (Cys-Cys-A$\beta_{1\text{-}40}$, or CC- A$\beta_{1\text{-}40}$) first forms spherical aggregates and then fibrils, creating *in trans* tetra-cysteine binding sites for FlAsH binding and fluorescence. EDT = 1,2-ethanedithiol, TCEP = tris(2-carboxyethyl)phosphine (**b**) Aggregation time courses of initially monomeric A$\beta_{1\text{-}40}$ or CC-A$\beta_{1\text{-}40}$ monitored by ThT fluorescence. The inset shows AFM images of CC-A$\beta_{1\text{-}40}$ fibrils and A$\beta_{1\text{-}40}$ fibrils. Scale bar = 250 nm. AFM images are shown in amplitude mode. (**c**) Monomeric CC-A$\beta_{1\text{-}40}$ (10 μM) or fibrillar CC-A$\beta_{1\text{-}40}$ was incubated with FlAsH-EDT$_2$ (100 μM) for 1 h at 25 °C. After removing unbound FlAsH-EDT$_2$, FlAsH fluorescence was measured (ex. 508 nm). The inset shows non-detectable binding of FlAsH to monomeric CC-A$\beta_{1\text{-}40}$, monomeric A$\beta_{1\text{-}40}$, and fibrillar A$\beta_{1\text{-}40}$. Representative figures of at least three different experiments are shown.

Author Manuscript Author Manuscript Author Manuscript Author Manuscript

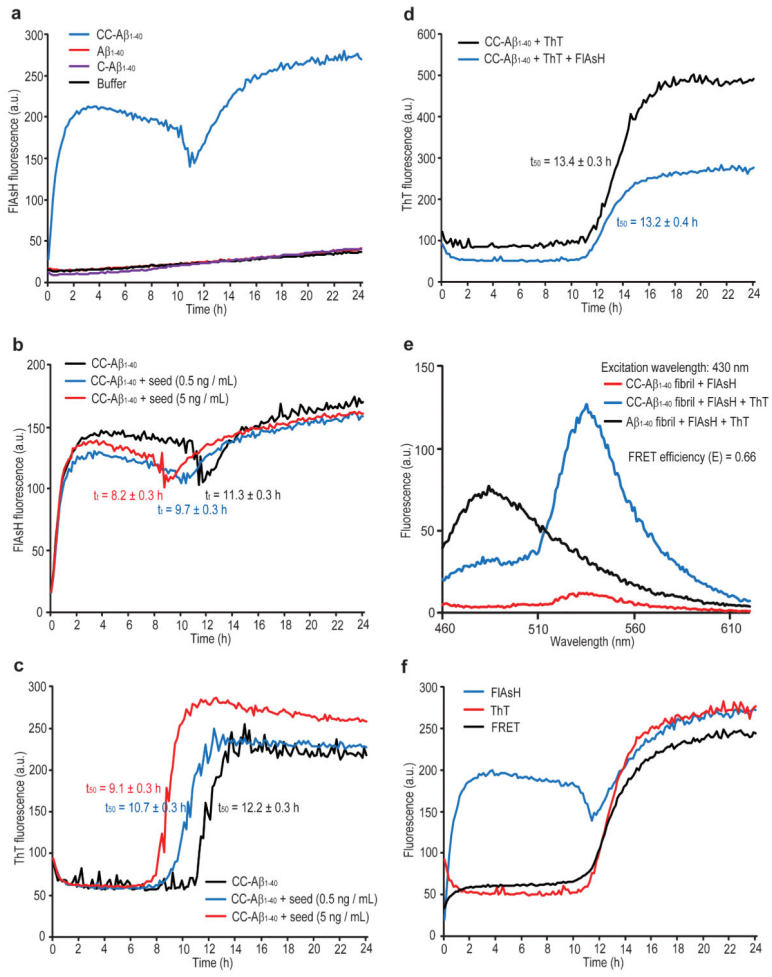

Figure 2.

Monitoring $A\beta_{1\text{-}40}$ aggregation by FlAsH, ThT, and ThT-to-FlAsH fluorescence resonance energy transfer (FRET). (**a**) Monomerized $A\beta_{1\text{-}40}$, C-$A\beta_{1\text{-}40}$, or CC-$A\beta_{1\text{-}40}$, (10 μM) was incubated with FlAsH-EDT_2 (0.5 μM) in 96-well plate at 37 °C. FlAsH fluorescence (Ex. 508 nm, Em. 560 nm) was measured every 10 min after shaking for 5 sec. (**b**) and (**c**) Monomerized CC-$A\beta_{1\text{-}40}$ (10 μM) was incubated with FlAsH-EDT_2 (0.5μM) or ThT (20 μM) in the absence or presence of variable seed ($A\beta_{1\text{-}40}$ fibril) concentrations and aggregation was monitored by FlAsH (**b**) or ThT (**c**, Ex. 430 nm, Em. 485 nm) fluorescence. t_t = the time of the second FlAsH-based transition, t_{50} = the time required for fibril formation to reach 50% completion. (**d**) Monomerized CC-$A\beta_{1\text{-}40}$ (10 μM) was incubated with ThT (20 μM) in the absence or presence of FlAsH-EDT_2 (0.5 μM) and ThT fluorescence was monitored. (**e**) Emission spectra (430 nm excitation) of CC-$A\beta_{1\text{-}40}$ or $A\beta_{1\text{-}40}$ (10 μM) incubated with FlAsH (0.5 μM) and ThT (20 μM). ThT emission λ_{max} = 485 nm. FlAsH emission λ_{max} = 530 nm. FRET efficiency (E) was obtained by measuring the fluorescence intensities of the donor with acceptor (IThT FlAsH) and without acceptor (I_{ThT}). $E = 1 - I_{ThT\ FlAsH} / I_{ThT}$ (**f**) Monomerized CC-$A\beta_{1\text{-}40}$ (10 μM) was incubated with ThT (20 μM) and FlAsH-EDT_2 (0.5 μM). FlAsH fluorescence, ThT fluorescence, and ThT-to-FlAsH FRET (Ex. 430 nm, Em. 560 nm) were monitored using the indicated excitation

Author Manuscript Author Manuscript Author Manuscript Author Manuscript

and emission wavelengths. Representative figures from at least three different experiments carried out in triplicate are shown.

Author Manuscript Author Manuscript Author Manuscript Author Manuscript

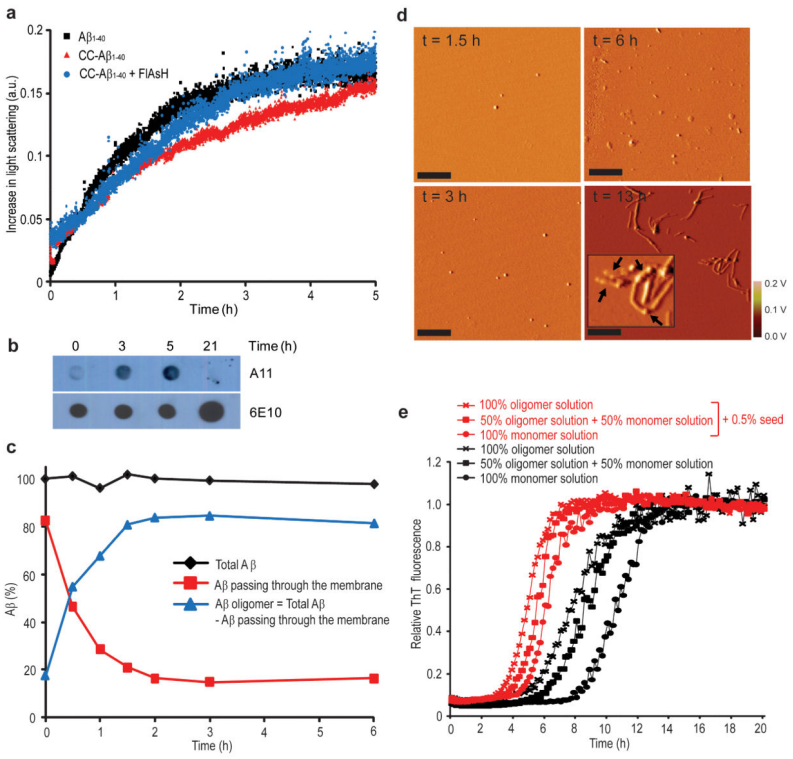

Figure 3.

CC-A$\beta_{1\text{-}40}$ aggregates by a nucleated conformational conversion mechanism. (**a**) Aggregation time course of monomerized CC-A$\beta_{1\text{-}40}$ or A$\beta_{1\text{-}40}$ (10 μM) monitored by measuring light scattering at 90°. (**b**) Dot-blot analysis of monomerized CC-A$\beta_{1\text{-}40}$ (10 μM) incubated at 37 °C in a plate reader for the indicated times. A11 is an oligomer selective antibody and 6E10 binds to most A$\beta_{1\text{-}40}$ aggregate morphologies. (**c**) The amount of CC-A$\beta_{1\text{-}40}$ before (total CC-A$\beta_{1\text{-}40}$) or after (filtered CC-A$\beta_{1\text{-}40}$) filtration through a 50kDa MW cut-off membrane during incubation at 37 °C in a plate reader. Each data point represents the average of at least 3 measurements. (**d**) AFM analysis of CC-A$\beta_{1\text{-}40}$ (10 μM) removed from an aggregation reaction at the indicated times. Arrows within the inset indicate assembly of oligomer units at the end of a fibril at t = 13 h. Scale bar = 500 nm. AFM images are shown in amplitude mode. (**e**) Monomeric A$\beta_{1\text{-}40}$ (10 μM) pre-incubated for 3.5 h in a plate reader at 37 °C with shaking for 5 sec every 10 min was designated as 100% oligomer solution (note the actual yield of oligomer formation is close to 85% (**Fig. 3c**)). This oligomer solution was used directly or mixed with various amount of freshly monomerized A$\beta_{1\text{-}40}$ solution (10 μM), and fibril formation of A$\beta_{1\text{-}40}$ was monitored in the absence or presence of seeds (0.5 %) by ThT binding fluorescence. Representative figures from at least three different experiments carried out in triplicate are shown.

Author Manuscript Author Manuscript Author Manuscript Author Manuscript

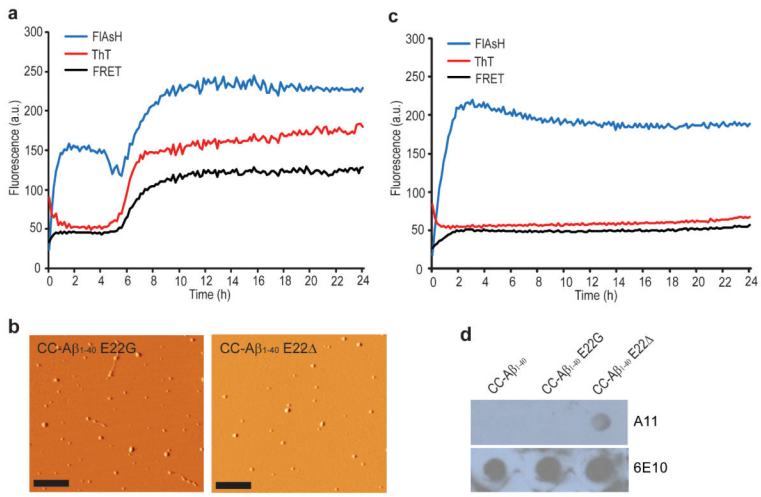

Figure 4.

Familial Alzheimer's mutant $A\beta_{1\text{-}40}$ aggregation time courses. Monomerized CC-$A\beta_{1\text{-}40}$ E22G (**a**) or CC-$A\beta_{1\text{-}40}$ E22Δ (**b**) (10 μM) was incubated with FlAsH-EDT_2 and ThT at 37 °C in a 96-well plate. FlAsH fluorescence (Ex. 508 nm, Em. 560 nm), ThT fluorescence (Ex. 430 nm, Em. 485 nm), and ThT-to-FlAsH FRET (Ex. 430 nm, Em. 560 nm) were measured every 10 min immediately following shaking for 5 sec. (**c**) A dot-blot assay was performed using the oligomer selective antibody A11 to assess the presence of soluble oligomers 24 h into the aggregation time course. (**d**) AFM analysis of CC-$A\beta_{1\text{-}40}$ E22G (left panel), or CC-$A\beta_{1\text{-}40}$ E22Δ (right panel) 24 h into the aggregation time course. Scale bar = 500 nm. Representative figures from at least three different experiments carried out in triplicate are shown.

Author Manuscript Author Manuscript Author Manuscript Author Manuscript

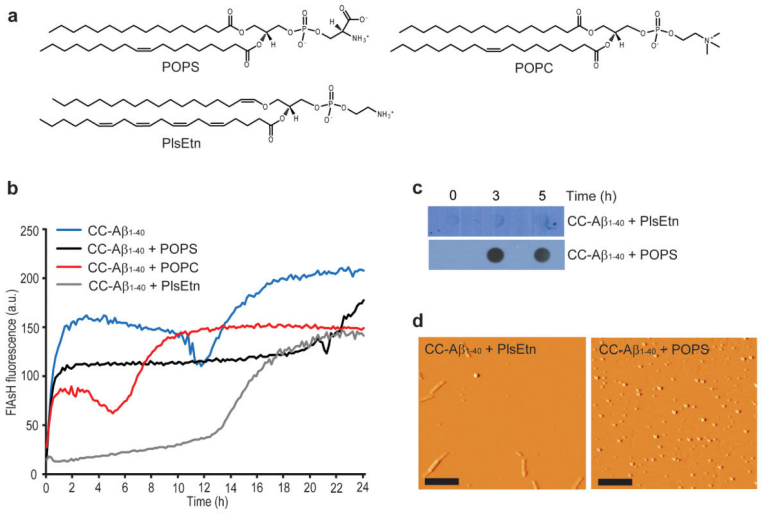

Figure 5.

Effect of large unilamellar vesicles (LUVs) comprising various lipids on Aβ aggregation. (**a**) Chemical structures of phospholipids investigated. POPS: 1-palmitoyl-2-oleoyl-*sn*-glycero-3-phospho-L-serine, POPC: 1-palmitoyl-2-oleoyl-*sn*-glycero-3-phosphocholine, PlsEtn: 1-(1Z-octadecenyl)-2-arachidonoyl-*sn*-glycero-3-phosphoethanolamine. (**b**) Monomerized CC-A$\beta_{1\text{-}40}$ (10 μM) was incubated at 37 °C with LUVs made of the indicated lipids (80 μM monomer concentration) and FlAsH fluorescence was monitored. For ThT fluorescence and ThT-to-FlAsH FRET see Supplementary Fig. 3. (**c**) Samples were removed at 0, 3, and 5 h from a CC-A$\beta_{1\text{-}40}$ / LUV aggregation assay to perform dot-blot using the A11 oligomer selective antibody. (**d**) Samples from a CC-A$\beta_{1\text{-}40}$ / PlsEtn aggregation assay (left panel) or a CC-A$\beta_{1\text{-}40}$ / POPS aggregation assay (right panel) were removed 18 h into the time course for AFM analysis. Scale bar = 500 nm. Representative figures of at least three different experiments carried out in triplicate are shown.

Author Manuscript Author Manuscript Author Manuscript Author Manuscript

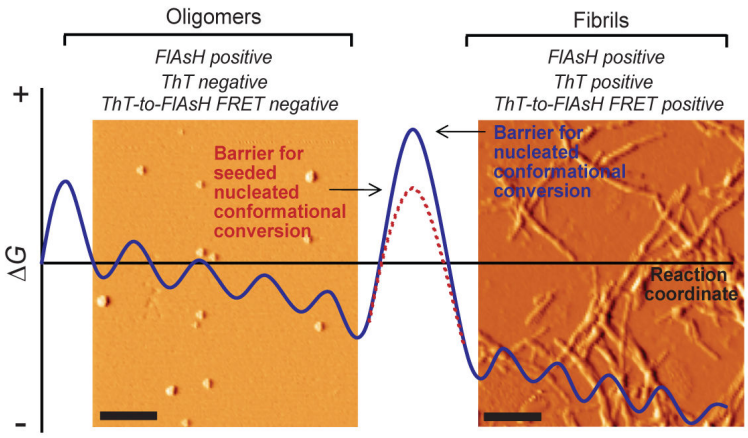

Figure 6.

Free-energy diagram for an $A\beta_{1\text{-}40}$ aggregation reaction proceeding by a nucleated conformational conversion mechanism. AFM images illustrate different kinds of aggregates form including oligomers before nucleated conformation conversion and fibrils after nucleated conformational conversion during aggregation of CC-$A\beta_{1\text{-}40}$ (scale bar = 250 nm).

Author Manuscript Author Manuscript Author Manuscript Author Manuscript

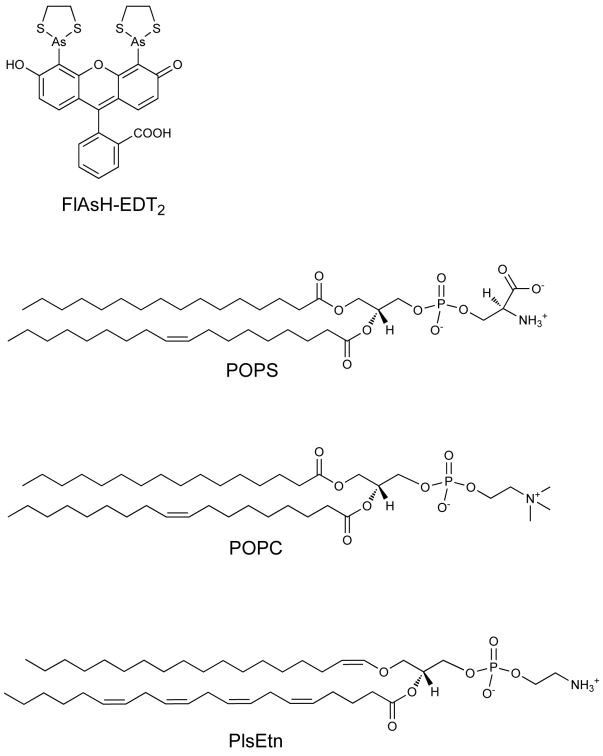

Figure 7.